nature cell biology

A role for Rho GTPases and cell–cell adhesion in single-cell motility *in vivo*

Elena Kardash[1], Michal Reichman-Fried[1], Jean-Léon Maître[2], Bijan Boldajipour[1], Ekaterina Papusheva[2], Esther-Maria Messerschmidt[1], Carl-Philipp Heisenberg[2] and Erez Raz[1,3]

Cell migration is central to embryonic development, homeostasis and disease[1], processes in which cells move as part of a group or individually. Whereas the mechanisms controlling single-cell migration *in vitro* are relatively well understood[2–4], less is known about the mechanisms promoting the motility of individual cells *in vivo*. In particular, it is not clear how cells that form blebs in their migration use those protrusions to bring about movement in the context of the three-dimensional cellular environment[5,6]. Here we show that the motility of chemokine-guided germ cells within the zebrafish embryo requires the function of the small Rho GTPases Rac1 and RhoA, as well as E-cadherin-mediated cell–cell adhesion. Using fluorescence resonance energy transfer we demonstrate that Rac1 and RhoA are activated in the cell front. At this location, Rac1 is responsible for the formation of actin-rich structures, and RhoA promotes retrograde actin flow. We propose that these actin-rich structures undergoing retrograde flow are essential for the generation of E-cadherin-mediated traction forces between the germ cells and the surrounding tissue and are therefore crucial for cell motility *in vivo*.

Guided by the chemokine CXCL12a/SDF-1a, zebrafish germ cells migrate as individual cells from the site at which they are specified to the site where the gonad develops[7–9]. During their migration, germ cells extend spherical cellular protrusions termed blebs, which are driven by actomyosin cortex contraction and hydrostatic pressure[5,6,10]. As a guiding chemokine, CXCL12a directs the formation of blebs, thereby polarizing the cell with respect to the source of the attractant cue[10]. In the absence of chemokine signalling, germ cells nevertheless migrate, albeit non-directionally, by polarizing and migrating in a random direction. Although a significant number of the molecules involved in generating the CXCL12-encoded directional information[8,11] and its interpretation[10] have been identified, the mechanisms responsible for the actual motility of zebrafish germ cells and of other cell types that use blebs in their migration are currently unknown. In particular, the mechanisms by which traction forces are generated to facilitate the bleb-assisted movement of cells relative to the surrounding tissue have not been defined[6].

To determine the molecular mechanisms controlling germ-cell motility, we first examined the dynamics of the actin cytoskeleton in cells and studied the function of members of the Rho family of GTPases[12,13] in this context. As described previously[10], we observed preferential accumulation of filamentous actin (F-actin) structures, which we refer to as 'brushes', at the leading edge of migrating polarized cells (Fig. 1a and Supplementary Information, Fig. S1a). A flow of cytosol into the expanding blebs advances the cell front beyond the actin-rich domain and is concurrent with backward movement of the actin ('run' in Fig. 1a and Supplementary Information, Movie S1). These events are followed by the formation of brushes at the new leading edge. Actin brushes are not found in cells in the course of 'tumbling' phases during which germ cells lose their polarity and do not migrate (ref. 9; 'tumbling' in Fig. 1a and Supplementary Information, Movie S1). This finding implies that the function of these structures is relevant to cell motility. An attractive candidate responsible for the production of actin brushes at the front of migrating cells is the Rho GTPase Rac1, which is an important regulator of actin cytoskeleton dynamics[12,13] and is uniformly expressed in zebrafish embryos in the relevant stages (Supplementary Information, Fig. S1b). To test this idea, we sought to determine the effect of altered Rac1 activity levels in germ cells on the formation of actin brushes. Specifically, we lowered Rac activity in germ cells by expressing the Cdc42/Rac interactive binding (CRIB) domain of PAK1 targeted to the membrane. Conversely, we increased Rac activity by expressing the constitutively active form, $Rac1^{V12}$. Decreasing the activity of Rac resulted in a strong inhibition of brush formation and a loss of cell polarity, effectively inhibiting the 'run' phase during which germ cells actively migrate (ref. 9; Fig. 1b and Supplementary Information, Movie S2). In contrast, extensive formation of multiple actin-rich structures was observed in $Rac1^{V12}$-expressing germ cells. These cells failed to form blebs, presumably as a result of inhibition of actomyosin contraction under these conditions (for example, by interference with proper contractile cortex formation[14]) (Fig. 1c and Supplementary Information,

[1]Institute for Cell Biology, Center for Molecular Biology of Inflammation, Von-Esmarch-Strasse 56, D-48149 Münster, Germany. [2]Max Planck Institute of Molecular Cell Biology and Genetics, Pfotenhauerstrasse 108, 01307 Dresden, Germany.
[3]Correspondence should be addressed to E.R. (e-mail: erez.raz@uni-muenster.de)

Received 31 July 2009; accepted 16 November 2009; published online 13 December 2009; DOI:10.1038/ncb2003.

© 2010 Macmillan Publishers Limited. All rights reserved.

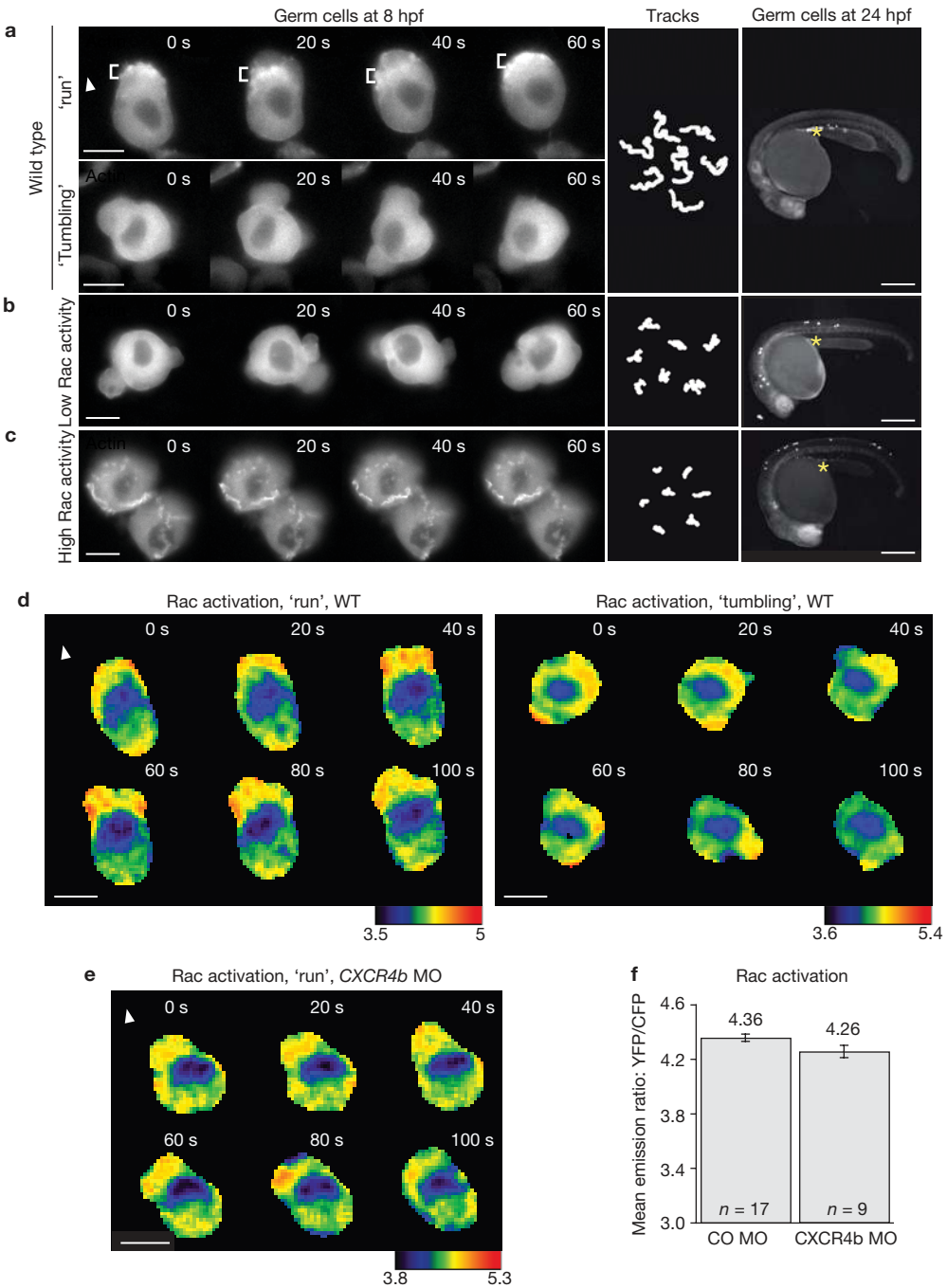

Figure 1 Actin cytoskeleton dynamics and Rac activity and function during germ-cell migration. (**a**–**c**) Actin in the germ cells was revealed in transgenic embryos expressing *EGFP–actin-nos1-3′ UTR* under the control of the *askopos* promoter[25]. (**a**) High-magnification snapshots (left panel) from a movie showing actin cytoskeleton dynamics in wild-type germ cells during 'run' and 'tumbling' phases. Brackets demarcate the actin brushes during 'run'. Numbers indicate time in seconds. Middle panel: migration tracks of germ cells. Right panel: germ cells located at the site where the gonad develops in the wild-type embryo at 24 hours after fertilization (hpf). (**b**) Actin cytoskeleton dynamics, migration tracks and position relative to the migration target of germ cells in which Rac activity is decreased by expression of the CRIB domain of PAK1 targeted to the membrane. (**c**) Actin cytoskeleton dynamics, migration tracks and position relative to the migration target of germ cells in which Rac activity is elevated by expression of the constitutively active form of Rac, $Rac1^{V12}$. (**d**) Rac activity in migrating wild-type (WT) germ cells expressing the cytosolic RacFRET biosensor at 8 hpf during 'run' (left panels) and 'tumbling' (right panels) phases. Ratio images of yellow fluorescent protein (YFP)/cyan fluorescent protein (CFP) emission for each cell are shown. (**e**) Rac activity in germ cells in which CXCR4b was knocked down. MO, morpholino. (**f**) Average activation level of Rac (mean emission ratio of YFP/CFP for the entire cell) in germ cells lacking CXCR4b signalling (right bar) compared with that in control cells (left bar). Track recording in **a**–**c** started at 7 hpf and spanned 70 min of migration. Data are mean ± s.e.m. Arrowheads in **a**, **d** and **e** indicate the direction of migration. Asterisks in **a**, **b** and **c** mark the migration target of the cells, the region where the gonad develops. Scale bars, 10 μm for high-magnification images and 300 μm for low-magnification images.

Movie S3). Consistent with the notion that proper regulation of actin brush formation is essential for normal germ-cell polarity and motility, germ cells in which Rac activity is deregulated have severe migration defects. In contrast with control cells, which migrated actively to arrive

© 2010 Macmillan Publishers Limited. All rights reserved.

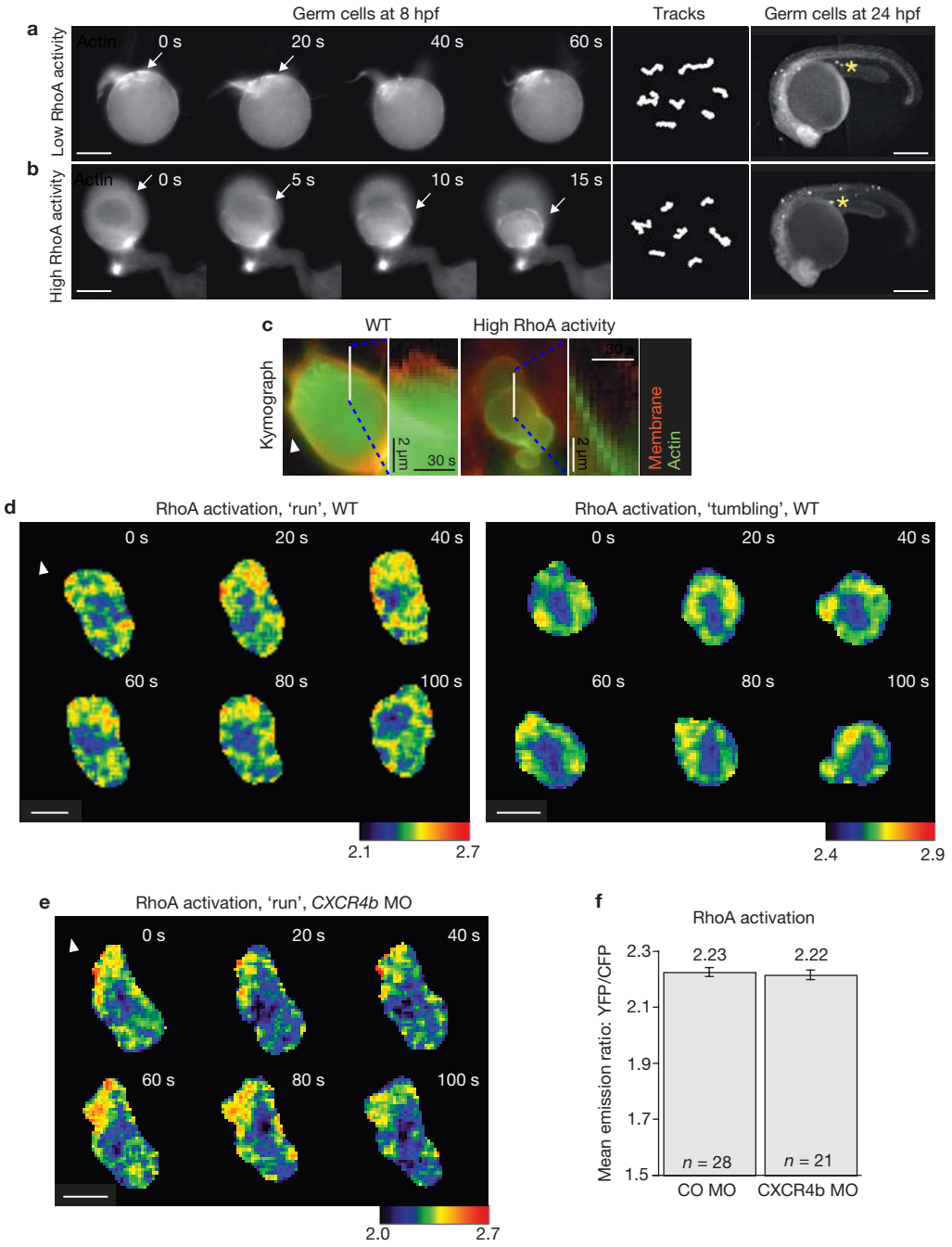

Figure 2 RhoA activity and role in regulating actin cytoskeleton dynamics in migrating germ cells. (**a**) Actin distribution (left panels), migration tracks (middle panel) and position relative to the migration target (right panel) of germ cells with a decreased level of the RhoA activity resulting from expression of the Rho-binding domain of protein kinase N targeted to the membrane. The arrow points at a stationary actin brush. Numbers indicate time in seconds. (**b**) Actin distribution (left panels), migration tracks (middle panel) and position relative to the migration target (right panel) of germ cells in which RhoA activity was enhanced by expressing the constitutively active form of RhoA, $RhoA^{V14}$. The arrow follows actin flow towards the back of the cell (see also Supplementary Information, Fig. S7). (**c**) Kymographs of actin retrograde flow in a wild-type (WT) germ cell (left) and in the germ cell expressing the activated $RhoA^{V14}$ protein (right). (**d**) RhoA activity in migrating wild-type germ cells expressing the cytosolic RhoA FRET biosensor at 8 hpf during 'run' (left panels) and 'tumbling' (right panels) phases. Ratio images of YFP/CFP are shown. (**e**) RhoA activity in germ cells in which CXCR4b was knocked down. MO, morpholino. (**f**) Average activation level of RhoA (mean emission ratio of YFP/CFP for the entire cell) in germ cells lacking CXCR4b signalling (right bar) compared with that of the wild type (left bar). Track recording in **a** and **b** started at 7 hpf and spanned 70 min of migration. Data are mean ± s.e.m. Arrowheads in **c**, **d** and **e** indicate the direction of migration. Asterisks in **a** and **b** mark the migration target of the germ cells, the region where the gonad develops in 24 hpf embryos. Scale bars, 10 μm for high-magnification images and 300 μm for low-magnification images.

at the site where the gonad develops (asterisk in Fig. 1a), germ cells in which Rac activity was manipulated showed short migration tracks and did not reach their target (Fig. 1b, c).

The results presented above suggest that controlling the amount and distribution of the actin brushes within cells is important for proper cell migration, and raise the possibility that Rac controls these aspects. To

© 2010 Macmillan Publishers Limited. All rights reserved.

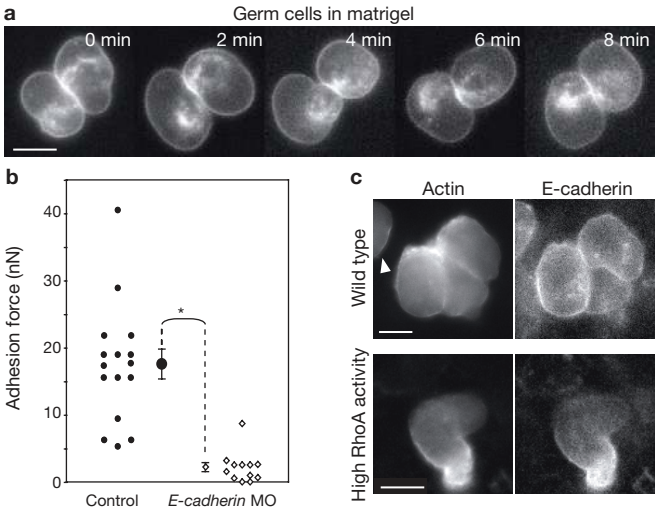

Figure 3 Cell–cell adhesion in germ-cell migration. (**a**) Snapshots from a movie showing the behaviour of germ cells placed in Matrigel. The membrane is revealed by expression of farnesylated enhanced green fluorescent protein (EGFP). Numbers indicate time in minutes. (**b**) Measurements of adhesion force between the individual pairs of germ cells and mesodermal cells in control embryos (filled circles) and in embryos knocked down for E-cadherin (open diamonds). MO, morpholino. The difference between the two data sets is significant (asterisk, $P < 10^{-5}$) by *t*-test. (**c**) The localization of actin (left panels, revealed by Lifeact-Ruby) and of E-cadherin (right panels, revealed by E-cadherin–GFP) in control cells (upper panels) and in cells expressing $RhoA^{V14}$ (lower panels). Scale bar, 10 μm. Arrowhead indicates migration direction.

examine whether the spatial distribution of Rac activity is correlated with positioning of the actin brushes, we monitored the activation pattern of Rac in migrating germ cells within the developing embryo by using a fluorescence resonance energy transfer (FRET)-based sensor (a modified version of the construct described in ref. 15; Supplementary Information, Fig. S2). Indeed, Rac activity was found to be elevated at the leading edge of actively migrating ('run') cells, while showing only transient unstable polarity in 'tumbling' cells (Fig. 1d and Supplementary Information, Fig. S3a and Movies S4 and S5). Persistent Rac activation is thus correlated with actin brush formation (Supplementary Information, Fig. S3c). Significantly, in germ cells that lack the CXCL12a receptor CXCR4b and thus migrate non-directionally, brushes were normally formed (Supplementary Information, Fig. S4a and Movie S6) and Rac activation levels (Fig. 1e, f) were normal. These results are consistent with the idea that polarized activation of Rac is primarily relevant for general cell motility rather than for directionality. Indeed, a local increase in the level of intracellular Ca^{2+}, a second messenger involved in transmitting directional information and defining the site of bleb formation[10], had no effect on the site of brush formation (Supplementary Information, Fig. S4b). Taken together, these results suggest that actin brushes are an important feature of polarized migrating cells.

To elucidate the function of the brushes, we examined the role of another Rho GTPase family member, RhoA, which is known to regulate cell motility and is uniformly expressed in zebrafish embryos during the relevant stages (Supplementary Information, Fig. S1b). This protein signals through effector proteins such as ROCK1 to enhance actomyosin contractility, and it has been implicated in myosin activation and retraction of the back of the cell during migration[3]. Accordingly, RhoA was shown to be activated at the back of cells[16], and antagonistic interactions between Rac and RhoA were reported (for example, in ref. 17). Recent studies, however, have also demonstrated RhoA activation at the front of cells migrating *in vitro*[18,19], suggesting that RhoA could exert additional functions in migrating cells other than retraction of the back of the cell. To assess the function of RhoA in germ-cell migration, we manipulated RhoA signalling and examined the effect of this on actin dynamics and cell behaviour. We subsequently determined where RhoA is activated.

We decreased RhoA activity by expressing the Rho-binding domain of protein kinase N targeted to the membrane of the germ cells and increased RhoA signalling by expressing the constitutively active version, $RhoA^{V14}$. Cells in which RhoA activity was decreased formed no blebs, presumably as a result of the decrease in myosin activity that is required for bleb formation[10]. In these cells, the brushes appeared stationary and were confined to the periphery of the cell (Fig. 2a and Supplementary Information, Movie S7). In contrast, high RhoA activity led to a strongly enhanced retrograde flow of actin in comparison with that in control cells, resulting in an accumulation of actin at the back of the cell (Supplementary Information, Fig. S5) and a lower level of actin at the cell front (Fig. 2b, c and Supplementary Information, Movie S8). The abnormal dynamics of actin brushes was correlated with strong defects in germ-cell migration, because altering RhoA activity resulted in abnormal migration tracks and ectopic positioning of the cells at the end of the first day of development (Fig. 2a, b).

These findings raised the possibility that RhoA has a role in regulating the dynamics of the brushes at the cell front. To examine this notion, we monitored the distribution of RhoA activity in germ cells within the developing embryo by using a FRET sensor (a modified version of the construct described in ref. 20; Supplementary Information, Fig. S6). In addition to activation domains detected at the back of migrating cells, polarized germ cells showed prominent RhoA activation at the leading edge (Fig. 2d and Supplementary Information, Fig. S3b). Consistent with the idea that polarized RhoA activity has a role in germ-cell motility, non-migratory, 'tumbling' cells did not form a stable domain of RhoA activation (Fig. 2d). In a similar manner to Rac, the RhoA activation pattern and level were not dependent on chemokine signalling (Fig. 2e, f), showing that RhoA function is primarily important for general cell motility.

The correlation between proper Rac-dependent brush formation along with RhoA-dependent retrograde actin flow and the competence of the cells to reach their target indicates that the dynamics of these structures is crucial for cell migration. Indeed, actin retrograde flow has been implicated in cell motility *in vitro*, where it functions in generating traction forces between cells and the extracellular matrix (ECM)[2]. Recent *in vitro* studies demonstrated the involvement of RhoA and myosin in the generation of traction force[21,22]. To determine the nature of the interaction between the contractile forces exerted within the cells and the extracellular environment *in vivo*, we examined the distribution of molecules known to reside in focal adhesion complexes. We found that proteins normally localized to focal adhesion complexes in cell culture were not distributed in a pattern resembling such a structure. Rather, fusion proteins of green fluorescent protein (GFP) and paxillin or zyxin expressed in germ cells had a homogeneous cytoplasmic distribution (data not shown). To evaluate the possible interaction of germ cells with the ECM, we monitored the behaviour of isolated germ cells plated on dishes coated with collagen type I, fibronectin, laminin, poly-(D-lysine) and poly-(L-lysine) and followed their behaviour with the use of time-lapse movies. This examination revealed that while the cells were generating protrusions, they showed neither

© 2010 Macmillan Publishers Limited. All rights reserved.

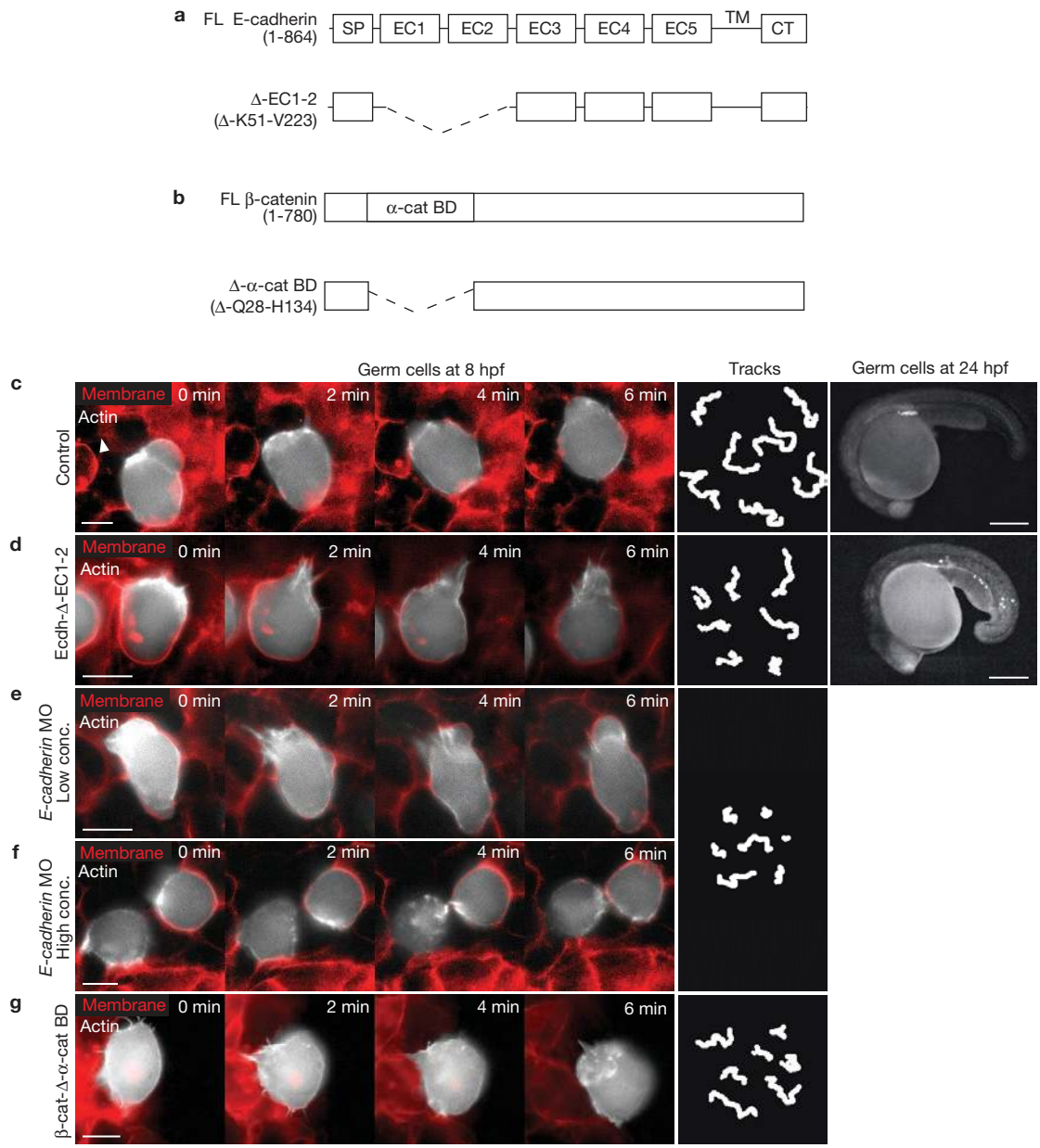

Figure 4 The role of E-cadherin in germ-cell migration. (**a**) The domain structure of E-cadherin and a schematic representation of the dominant-negative E-cadherin form used to interfere with E-cadherin function in germ cells. SP, signal peptide; EC, extracellular domain; TM, transmembrane domain; CT, cytoplasmic domain. (**b**) The domain structure of β-catenin and a schematic representation of the dominant–negative β-catenin form used to interfere with the coupling between E-cadherin and actin. BD, binding domain. (**c**–**g**) Left panels: expression of Lifeact–EGFP in germ cells (to show F-actin) and global expression of farnesylated mCherry (to show the cell membrane in red). Middle panels: 70-min tracks of germ cells migrating within embryos (recording started at 8 hpf). Right panels: the location of the germ cells in 24 hpf embryos. (**c**) Control germ cell. (**d**) Germ cells expressing the Δ-EC1-2 E-cadherin mutant version. The cells form brushes but show strong inhibition of migration. (**e**) Germ cells in embryos injected with a low concentration (30 pg per embryo) of anti-E-cadherin morpholinos (MO). The cells polarize and form brushes that undergo retrograde flow, but are unable to move relative to the somatic environment. (**f**) Germ cells in embryos injected with a high concentration (100 pg per embryo) of anti-E-cadherin morpholinos. The cells do not polarize or migrate and show severe defects in brush organization. (**g**) Germ cells expressing the β-catenin dominant-negative version. Such cells are unable to polarize or migrate properly, and brush organization appears disrupted. Embryos in **e**–**g** do not survive to the 24 hpf stage. Scale bars, 10 μm for high-magnification images and 300 μm for low-magnification images. Arrowhead indicates migration direction.

motility nor adhesion to those surfaces (data not shown). Furthermore, germ cells failed to migrate when plated in Matrigel, which provided a three-dimensional ECM environment, while showing extensive non-directional formation of blebs (Fig. 3a and Supplementary Information, Movie S9). Consistent with the results presented above, simultaneous knockdown of both zebrafish integrin β1a and integrin β1b, the only integrin β1 paralogues whose RNA is expressed at the relevant stages[23], did not prevent germ cells from reaching their target (Supplementary Information, Fig. S7a, b). Similar results were obtained on exposure to RGD peptide to inhibit integrin function. Despite the deleterious effect of these treatments on the general morphology of somatic tissues, the germ cells formed clusters at the site of the gonad (Supplementary Information,

© 2010 Macmillan Publishers Limited. All rights reserved.

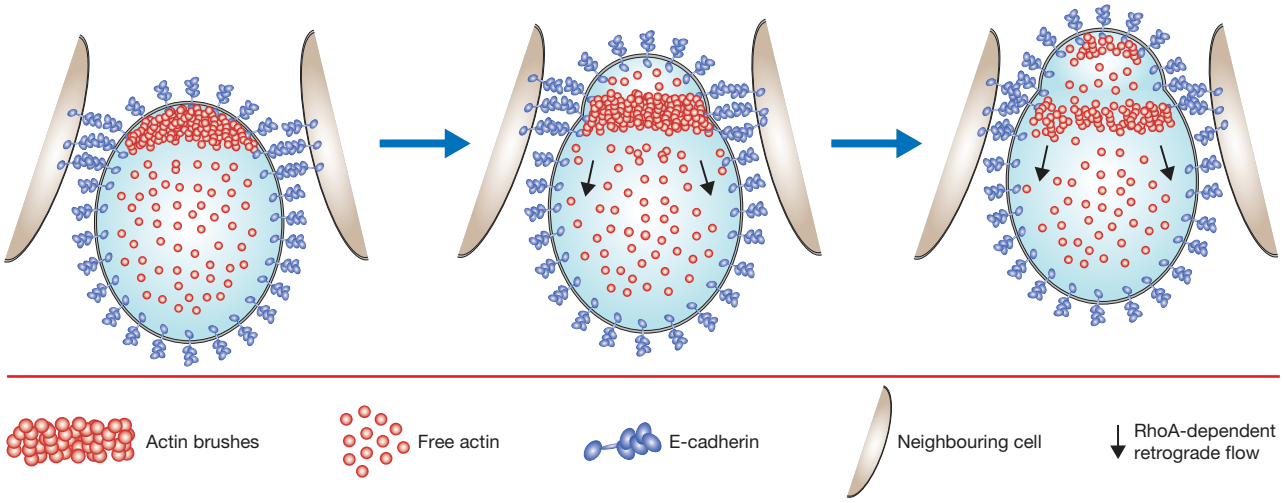

Figure 5 A model for cooperation between blebbing, actin retrograde flow and E-cadherin-mediated traction force in germ-cell motility. E-cadherin molecules (blue) are linked to actin brushes (red) that are enriched at the cell front. RhoA-enhanced retrograde flow (black arrows) allows the generation of traction forces. During blebbing, the cell is anchored to neighbouring cells by E-cadherin; the cell front advances rapidly, generating a new platform for brush formation ahead of the previous cell front.

Fig. S7b). Moreover, the migration tracks (and therefore the speed) of cells migrating in an environment compromised for integrin-β1 function were similar to those of cells migrating in control embryos (Supplementary Information, Fig. S7c). Taken together, these findings do not provide any supporting evidence that germ-cell–ECM interaction has an obligatory role in promoting germ-cell motility.

Whereas germ cells do not seem to use the ECM for their migration, they adhere to each other (Fig. 3a and Supplementary Information, Movie S9), suggesting that cell–cell adhesion might be an essential constituent of germ cells' interaction with their environment. Indeed, germ cells migrating within the embryo are intimately associated with neighbouring cells (Fig. 4c and Supplementary Information, Movie S10), presenting the possibility that the cell adhesion molecule E-cadherin has a role in this process[24]. Along these lines, the generation of blebs by recently specified germ cells is insufficient to promote cell movement[25], suggesting that the interaction with the cellular environment has to be altered for motility to occur. Indeed, the level of E-cadherin expressed on the surface of germ cells was shown to be mildly reduced at the time that germ cells initiated their migration. Consistently, zebrafish germ cells expressing abnormally high levels of E-cadherin migrated more slowly, suggesting that fine regulation of the protein level on the cell surface is important for proper motility[25,26]. To examine whether E-cadherin is involved in the interaction of germ cells with the environment, we measured the adhesion force between germ cells and somatic cells isolated from wild-type embryos or from embryos in which E-cadherin function had been knocked down, resulting in decreased levels of this molecule on the cell surface (data not shown). In the absence of E-cadherin, the adhesion between germ cells and somatic cells was markedly decreased (Fig. 3b), suggesting that this adhesion molecule has a major role in mediating the interaction between these cell populations. To examine the distribution of E-cadherin relative to that of actin, we expressed a GFP-tagged version of E-cadherin and compared its localization with that of F-actin. Similarly to our findings in fixed embryos[25], E-cadherin uniformly decorated the cell membrane of live germ cells (Fig. 3c and Supplementary Information, Movie S11). To determine whether actin brushes could be linked to E-cadherin, we analysed the distribution of E-cadherin under conditions in which the brushes were experimentally concentrated at the back of the cell on increasing Rho activity (Fig. 2b). This manipulation led to a marked alteration in the distribution of E-cadherin–GFP molecules in the germ cells such that both actin brushes and E-cadherin accumulated at the back of the manipulated cells (Fig. 3c and Supplementary Information, Movie S12). This result argues for a link between the two molecules. It is therefore conceivable that actin retrograde flow in the brushes is coupled to E-cadherin and could thus generate traction forces at the front of migrating germ cells.

To determine the functional relevance of E-cadherin-mediated adhesion for germ-cell migration we interfered with its activity. We were able to affect E-cadherin function specifically in the germ cells by expressing a dominant-negative mutant form lacking the extracellular domains normally engaged in the homophilic interaction, while global levels of E-cadherin were decreased by using specific morpholino antisense oligonucleotides. In support of the idea that traction forces are mediated by E-cadherin, interfering with its activity in the germ cells or in the whole embryo affected the dynamics and organization of the actin brushes, and inhibited the motility of cells along with their ability to reach the target (Fig. 4d–f). Specifically, those treatments resulted in 'uncoupling' of the actin brushes, such that despite a normal production of blebs, normal cell polarization and normal actin retrograde flow, cell motility was strongly inhibited (migration tracks in Fig. 4d–f and Supplementary Information, Movies S13–S15). These results indicate that actin retrograde flow and blebbing alone are insufficient to drive motility in the absence of traction. It is noteworthy that a strong decrease in E-cadherin levels also interfered with brush formation, suggesting that brushes require E-cadherin for their proper organization (Fig. 4f and Supplementary Information, Movie S15). To further demonstrate the importance of the actin–E-cadherin interaction for germ-cell migration, we explored the role of β-catenin, a molecule involved in mediating this interaction[27,28]. Indeed, expressing a β-catenin version lacking the protein domain required for α-catenin binding[29] induced strong defects in germ-cell migration and interfered with proper brush formation (Fig. 4b, g). Taken together, these results suggest that the connection between E-cadherin and actin is essential for proper motility of cells.

© 2010 Macmillan Publishers Limited. All rights reserved.

Our findings show that Rac-dependent actin brush formation, Rho-dependent retrograde flow and coupling of the brushes to neighbouring cells through E-cadherin cooperate in generating traction forces required for motility (Fig. 5). We propose that the blebs at the leading edge serve as a strategy for the rapid forward translocation of the platform on which the actin brushes assemble and exert their function.

The mechanisms promoting cell migration *in vivo* involving the Rho GTPase-dependent E-cadherin-mediated traction described here could be relevant for a wide range of cell migration processes in normal development and disease. For example, E-cadherin level and distribution in *Drosophila* germ cells are tightly regulated during their migration[30]. There, too, cadherin levels on the cell surface are critical for the proper timing and quality of interaction with surrounding cells such that *Drosophila* germ cells with compromised E-cadherin function show increased dispersal[30], reminiscent of the decrease in E-cadherin in the early germ-cell cluster observed before the initiation of zebrafish germ-cell migration. Controlling E-cadherin levels is also important for the migration of cells that travel as a group, because $G\alpha_{12/13}$-regulated E-cadherin activity was shown to be essential for normal zebrafish gastrulation[31,32]. In addition, E-cadherin was shown to be important for cell-cluster migration in the case of border cells in the *Drosophila* ovary[33,34]. E-cadherin was also shown to be important for the metastasis of certain types of cancer, in which regulating the level of this molecule either within the tumour or in the environment promoted cell invasion (see refs 35, 36 for recent reports). Hence, the mechanisms facilitating germ-cell motility *in vivo* presented here provide a general framework for understanding other cell migration processes for which E-cadherin function is required. □

METHODS

Methods and any associated references are available in the online version of the paper at http://www.nature.com/naturecellbiology/.

Note: Supplementary Information is available on the Nature Cell Biology website.

ACKNOWLEDGEMENTS

The FRET biosensors for Rac and RhoA were a gift from M. Matsuda. The yellow variant of GFP, YPet, was generously provided by P. Daugherty. Lifeact fusions were a gift from R. Wedlich-Soldner, and the GFP-CLIP-170 was provided by Franck Perez. We thank Donna Arndt-Jovin and Tom Jovin for their help with the FRET experiments. This work is supported by grants from the Deutsche Forschungsgemeinschaft (DFG) and the Max Planck Society. E.K. and B.B. are students at the International Max Planck Research School, Göttingen.

AUTHOR CONTRIBUTIONS

E.K. performed all the experiments except for the following: the initial characterization of Rac and RhoA phenotypes, generation of enhanced green fluorescent protein–actin transgenic line, track analysis in Figs 1, 2 and 4 and Supplementary Information, Fig. S7c, and *in situ* analysis in Supplementary Information, Fig. S1b were performed by M.R.; cell behaviour in Matrigel was conducted by B.B., adhesion measurements were performed by J.-L.M. and C.-P. H.; and the experiment described in Supplementary Information, Fig. S7a was performed by E.P. and C.-P.H. E.M. cloned DNA constructs and performed RNA injections. E.K., M.R. and E.R. wrote the manuscript.

COMPETING FINANCIAL INTERESTS

The authors declare no competing financial interests.

Published online at http://www.nature.com/naturecellbiology
Reprints and permissions information is available online at http://npg.nature.com/reprintsandpermissions/

1. Horwitz, R. & Webb, D. Cell migration. *Curr. Biol.* **13,** R756–R759 (2003).
2. Lauffenburger, D. A. & Horwitz, A. F. Cell migration: a physically integrated molecular process. *Cell* **84,** 359–369 (1996).
3. Ridley, A. J. *et al.* Cell migration: integrating signals from front to back. *Science* **302,** 1704–1709 (2003).
4. Puklin-Faucher, E. & Sheetz, M. P. The mechanical integrin cycle. *J. Cell Sci.* **122,** 179–186 (2009).
5. Fackler, O. T. & Grosse, R. Cell motility through plasma membrane blebbing. *J. Cell Biol.* **181,** 879–884 (2008).
6. Charras, G. & Paluch, E. Blebs lead the way: how to migrate without lamellipodia. *Nature Rev. Mol. Cell Biol.* **9,** 730–736 (2008).
7. Kunwar, P. S., Siekhaus, D. E. & Lehmann, R. *In vivo* migration: a germ cell perspective. *Annu. Rev. Cell Dev. Biol.* **22,** 237–265 (2006).
8. Doitsidou, M. *et al.* Guidance of primordial germ cell migration by the chemokine SDF-1. *Cell* **111,** 647–659 (2002).
9. Reichman-Fried, M., Minina, S. & Raz, E. Autonomous modes of behavior in primordial germ cell migration. *Dev. Cell* **6,** 589–596 (2004).
10. Blaser, H. *et al.* Migration of zebrafish primordial germ cells: a role for myosin contraction and cytoplasmic flow. *Dev. Cell* **11,** 613–627 (2006).
11. Boldajipour, B. *et al.* Control of chemokine-guided cell migration by ligand sequestration. *Cell* **132,** 463–473 (2008).
12. Heasman, S. J. & Ridley, A. J. Mammalian Rho GTPases: new insights into their functions from *in vivo* studies. *Nature Rev. Mol. Cell Biol.* **9,** 690–701 (2008).
13. Jaffe, A. B. & Hall, A. Rho GTPases: biochemistry and biology. *Annu. Rev. Cell Dev. Biol.* **21,** 247–269 (2005).
14. Sanders, L. C., Matsumura, F., Bokoch, G. M. & de Lanerolle, P. Inhibition of myosin light chain kinase by p21-activated kinase. *Science* **283,** 2083–2085 (1999).
15. Itoh, R. E. *et al.* Activation of rac and cdc42 video imaged by fluorescent resonance energy transfer-based single-molecule probes in the membrane of living cells. *Mol. Cell. Biol.* **22,** 6582–6591 (2002).
16. Wong, K., Pertz, O., Hahn, K. & Bourne, H. Neutrophil polarization: spatiotemporal dynamics of RhoA activity support a self-organizing mechanism. *Proc. Natl Acad. Sci. USA* **103,** 3639–3644 (2006).
17. Sander, E. E., ten Klooster, J. P., van Delft, S., van der Kammen, R. A. & Collard, J. G. Rac downregulates Rho activity: reciprocal balance between both GTPases determines cellular morphology and migratory behavior. *J. Cell Biol.* **147,** 1009–1022 (1999).
18. Pertz, O., Hodgson, L., Klemke, R. L. & Hahn, K. M. Spatiotemporal dynamics of RhoA activity in migrating cells. *Nature* **440,** 1069–1072 (2006).
19. Kurokawa, K. & Matsuda, M. Localized RhoA activation as a requirement for the induction of membrane ruffling. *Mol. Biol. Cell* **16,** 4294–4303 (2005).
20. Yoshizaki, H. *et al.* Activity of Rho-family GTPases during cell division as visualized with FRET-based probes. *J. Cell Biol.* **162,** 223–232 (2003).
21. Gupton, S. L. & Waterman-Storer, C. M. Spatiotemporal feedback between actomyosin and focal-adhesion systems optimizes rapid cell migration. *Cell* **125,** 1361–1374 (2006).
22. Gardel, M. L. *et al.* Traction stress in focal adhesions correlates biphasically with actin retrograde flow speed. *J. Cell Biol.* **183,** 999–1005 (2008).
23. Mould, A. P. *et al.* Identification of multiple integrin β1 homologs in zebrafish (*Danio rerio*). *BMC Cell Biol.* **7,** 24 (2006).
24. Gumbiner, B. M. Regulation of cadherin-mediated adhesion in morphogenesis. *Nature Rev. Mol. Cell Biol.* **6,** 622–634 (2005).
25. Blaser, H. *et al.* Transition from non-motile behaviour to directed migration during early PGC development in zebrafish. *J. Cell Sci.* **118,** 4027–4038 (2005).
26. Mich, J. K. *et al.* Germ cell migration in zebrafish is cyclopamine-sensitive but Smoothened-independent. *Dev. Biol.* **328,** 342–354 (2009).
27. Kemler, R. From cadherins to catenins: cytoplasmic protein interactions and regulation of cell adhesion. *Trends Genet.* **9,** 317–321 (1993).
28. Nelson, W. J. Regulation of cell–cell adhesion by the cadherin–catenin complex. *Biochem. Soc. Trans.* **36,** 149–155 (2008).
29. Oyama, T. *et al.* A truncated β-catenin disrupts the interaction between E-cadherin and α-catenin: a cause of loss of intercellular adhesiveness in human cancer cell lines. *Cancer Res.* **54,** 6282–6287 (1994).
30. Kunwar, P. S. *et al.* Tre1 GPCR initiates germ cell transepithelial migration by regulating *Drosophila melanogaster* E-cadherin. *J. Cell Biol.* **183,** 157–168 (2008).
31. Kane, D. A., McFarland, K. N. & Warga, R. M. Mutations in half baked/E-cadherin block cell behaviors that are necessary for teleost epiboly. *Development* **132,** 1105–1116 (2005).
32. Lin, F. *et al.* $G\alpha_{12/13}$ regulate epiboly by inhibiting E-cadherin activity and modulating the actin cytoskeleton. *J. Cell Biol.* **184,** 909–921 (2009).
33. Geisbrecht, E. R. & Montell, D. J. Myosin VI is required for E-cadherin-mediated border cell migration. *Nature Cell Biol.* **4,** 616–620 (2002).
34. Fulga, T. A. & Rorth, P. Invasive cell migration is initiated by guided growth of long cellular extensions. *Nature Cell Biol.* **4,** 715–719 (2002).
35. Hogan, C. *et al.* Characterization of the interface between normal and transformed epithelial cells. *Nature Cell Biol.* **11,** 460–467 (2009).
36. Wang, S. P. *et al.* p53 controls cancer cell invasion by inducing the MDM2-mediated degradation of Slug. *Nature Cell Biol.* **11,** 694–704 (2009).

© 2010 Macmillan Publishers Limited. All rights reserved.

DOI: 10.1038/ncb2003

METHODS

Zebrafish strains. The Tol-kop-EGFP-F-nos1-3′UTR and the Tol-kop-DsRed-nos1-3′UTR transgenic fish line were described previously[11,25,26]. The Tol-kop-EGFP-zf β-actin-nos1-3′UTR transgenic fish line was generated in a similar way, exchanging the EGFP-F in the previous construct with an EGFP-zf β-actin fusion, permitting visualization of actin dynamics in the germ cells. For cell–cell adhesion measurements, germ cells and mesodermal cells were isolated from the embryos generated by crossing Tol-kop-dsRed-nos1-3′UTR transgenic females (labelling the germ cells in red) and goosecoid–GFP transgenic males (labelling mesodermal cells in green).

Plating germ cells on Matrigel. Embryos from Tol-kop-EGFP-F-nos1-3′UTR transgenic fish were dechorionated at 6 hpf and disrupted in phenol-red-free Matrigel (BD Bioscience) diluted to 50% with L-15 medium (Invitrogen). Matrigel was left to gel at 28 °C for 30 min and overlaid with L-15 medium. A Zeiss ImagerZ microscope was used to image cells up to 24 h after plating.

RNA expression constructs and injections. Capped sense RNA was synthesized with the mMessage mMachine kit (Ambion). To direct protein expression to PGCs, the open reading frames (ORFs) were fused upstream to the 3′ untranslated region (UTR) of the *nanos1* (*nos1-3′UTR*) gene, facilitating translation and stabilization of the RNA in these cells[37]. For global protein expression in the embryo, the ORFs were cloned into the pSP64TS vector between the 5′ and 3′ UTRs of the *Xenopus globin* gene. The injected RNA amounts for each construct are provided below. *mCherry-F-globin* (A709) labels the membranes in all cells and was injected at 90 pg per embryo. *Cytosolic Rac FRET* (A422) is a modified Rac FRET biosensor. The Venus in the original Rac FRET[15] was replaced with YPet[38], and the carboxy-terminal domain that follows SECFP in the original FRET construct was removed (Supplementary Information, Fig. S2b); the RNA was injected at 360 pg per embryo. Cytosolic *RhoA YPet FRET-nos1-3′UTR* (A676) is a modified RhoA FRET biosensor. The Venus in the original RhoA FRET[20] was replaced with YPet, and the most C-terminal domain that follows SECFP in the original FRET construct was removed (Supplementary Information, Fig. S6b); the RNA was injected at 360 pg per embryo.

hCRIB-RasCT-nos1-3′UTR (A820) contains the CRIB domain of human PAK1 from the RacFRET biosensor[15] fused to the farnesylation signal from the C-terminal tail of human Ras. The construct was used to inhibit Rac function in germ cells; its RNA was injected at 450 pg per embryo. *Rac1V12-nos1-3′UTR* (481) contains the constitutively active Rac1 and was generated by introducing a G12V substitution in the coding region of the zebrafish Rac1; the RNA was injected at 150 pg per embryo.

zRhoAV14-nos1-3′UTR (B282) contains the constitutively active RhoA and was generated by introducing a G14V substitution in the coding region of zebrafish RhoA; the RNA was injected at 30 pg per embryo. *YFP-hPKN-hRasCT-nos1-3′UTR* (A994) contains the Rho-binding domain of protein kinase N (PKN); the RNA was injected at 450 pg per embryo. *Abp140-17aaEGFP-nos1-3′UTR* (B006; Lifeact) and *Abp140-17aaRuby-nos1-3′UTR* (B007)[39] were used for labelling filamentous actin in germ cells in green and red, respectively, and were injected at 120 pg per embryo.

The dominant-negative E-cadherin construct *Cdh1-delEC1-2-nos1-3′UTR* (B394) lacks the first and second extracellular domains of the protein (deletion of amino acids K51-V223); the RNA was injected at 600 pg per embryo.

E-cadherin1-GFP-globin-3′UTR (B227) was used to reveal the localization of E-cadherin in germ cells and in somatic cells. The coding region of E-cadherin without a STOP codon was fused amino-terminally to GFP and to the *globin 3′UTR*; the RNA was injected at 300 pg per embryo. β-*catenin(del-Q28-H134)-nos1-3′UTR* (B605) contains the zebrafish β-*catenin* gene in which the sequence encoding amino acids Q28 to H134 was deleted as described previously[29]. The RNA was injected at 300 pg per embryo.

Morpholino knockdown experiments. To inhibit protein translation in the embryo, morpholino antisense oligonucleotides (Gene Tools) were injected into one-cell stage embryos. Control morpholino, 5′-CCTCTTACCTCAGTTACAATTTATA-3′; CXCR4b, 5′-AAATGATGCTATCGTAAAATTCCAT-3′, E-cadherin MO1, 5′-ATCCCACAGTTGTTACACAAGCCAT-3′; E-cadherin MO2, 5′–TAAATCGCAGCTCTTCCTTCCAACG-3′.

Dual micropipette aspiration assay. The dual micropipette aspiration assay was performed as described previously[40]. Cells were prepared from transgenic embryos whose mesodermal cells had been labelled with GFP and their germ cells with red fluorescent protein. Cells were isolated at 90% epiboly and manipulated at 25 °C with two micropipettes, each held by a micromanipulator connected to a microfluidic pump (Fluigent). Micropipettes with an internal diameter of 6–7 μm were pulled (model P-97; Sutter Instrument), cut, and fire-polished. Cells were imaged with an inverted epifluorescence microscope (Zeiss) equipped with a 40× objective (Zeiss LD PlanNeoFluar 0.6 numerical aperture Ph2 Korr) and a cooled charge-coupled device CoolSnap HQ (Photometrics); images were acquired with Metamorph software.

Fluorescent microscopy. Confocal fluorescence images of migrating germ cells were acquired with a Leica TCS SL2 or Zeiss LSM710 microscope. Epifluorescence images or time-lapse movies of migrating germ cells were generated on a Zeiss Axioplan2 or Zeiss ImagerZ upright microscope controlled by Metamorph software. For high-magnification imaging of cell morphology, 40× and 63× water-immersion objectives were used. For speed and track analysis of PGC migration, a 10× objective was used. Images were processed with ImageJ or Metamorph software. Time-lapse movies lasting 70 min were used for generating migration tracks as described previously[9].

FRET imaging and analysis. To measure Rac and RhoA activity, FRET ratio imaging was performed with the Zeiss Axioplan2 upright microscope in accordance with the Phogemon instructions (http://www.path1.med.kyoto-u.ac.jp/mm/e-phogemon/phomane.htm) and as described previously[15]. For each experiment, at least 50 cells were recorded in three independent experiments, using the same settings for image acquisition. To measure FRET, two emission images called CFP and YFP for donor and acceptor emission, respectively, were acquired upon donor excitation. A 440AF21 (XF1071; Omega optical) filter set was used for the donor excitation with 455DRLP as the dichroic mirror. The emissions were filtered with 480AF30 (XF3075; Omega optical) for the donor and 535AF26 (XF3079; Omega optical) for the acceptor. To reduce bleaching, a 6% neutral density filter was inserted before the ultraviolet pass. CFP and YFP images were acquired either sequentially using the switching wheel (Fig. 1d, e and Supplementary Information, Figs S2c, d and S3a) or simultaneously with the Dual-View (Fig. 2d, e and Supplementary Information, Figs S3b, c and S6c). With the switching wheel, to avoid possible artefacts the experiments were performed twice, with the order of recording YFP and CFP images alternated.

Ratio image generation algorithm. ImageJ software was used to generate ratio YFP/CFP images. The raw images were background corrected with a rolling-ball algorithm implemented in ImageJ. YFP images were registered with the TurboReg plugin, using CFP image as a reference; the smooth filter was then applied on both images. The YFP image was auto-thresholded, setting the background values to NaN (not a number). The ratio image was generated with the Ratio Plus plugin.

37. Köprunner, M., Thisse, C., Thisse, B. & Raz, E. A zebrafish nanos-related gene is essential for the development of primordial germ cells. *Genes Dev.* **15,** 2877–2885 (2001).
38. Nguyen, A. W. & Daugherty, P. S. Evolutionary optimization of fluorescent proteins for intracellular FRET. *Nature Biotechnol.* **23,** 355–360 (2005).
39. Riedl, J. *et al.* Lifeact: a versatile marker to visualize F-actin. *Nature Methods* **5,** 605–607 (2008).
40. Daoudi, M. *et al.* Enhanced adhesive capacities of the naturally occurring Ile249-Met280 variant of the chemokine receptor CX3CR1. *J. Biol. Chem.* **279,** 19649–19657 (2004).

© 2010 Macmillan Publishers Limited. All rights reserved.

nature cell biology

DOI: 10.1038/ncb2003

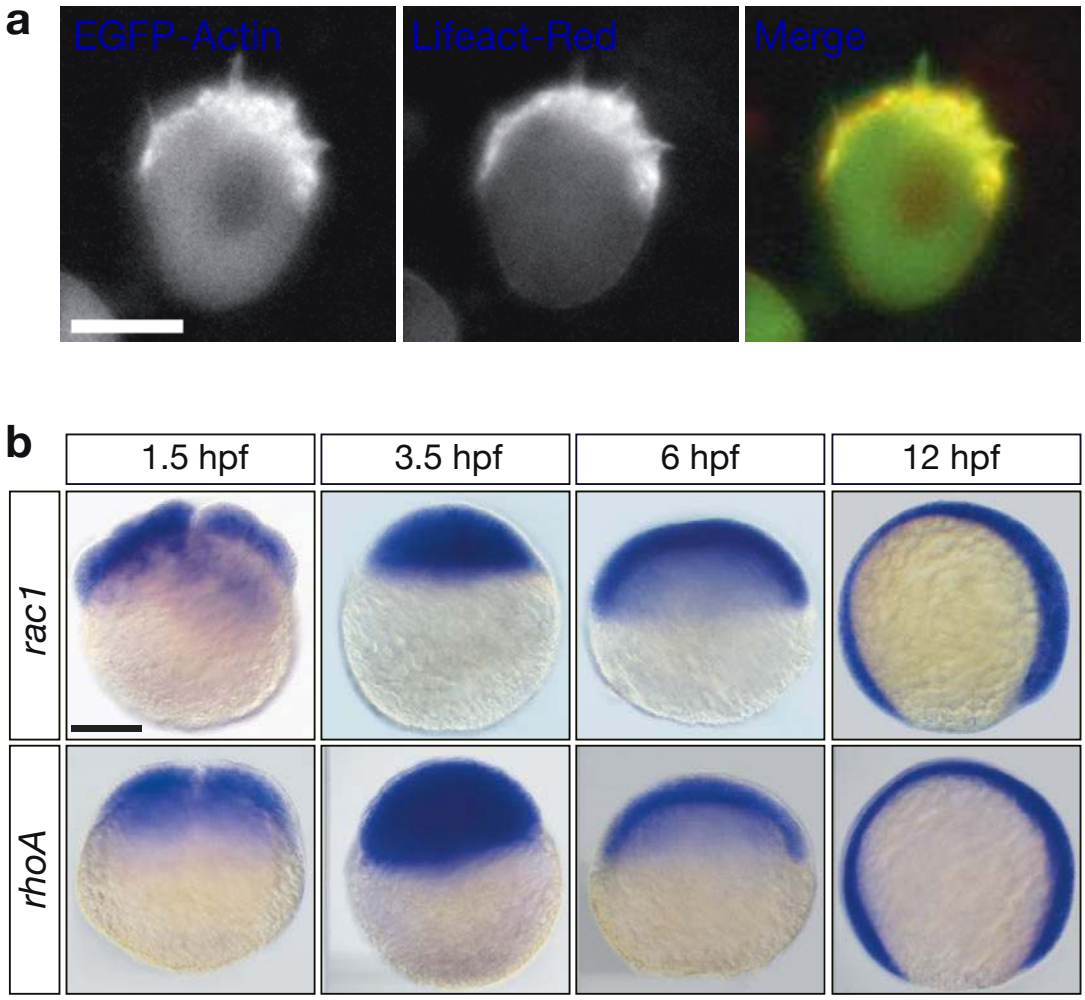

Figure S1 Distribution of F-actin in germ cells and the RNA expression pattern of *rac*1 and *rho*A in early zebrafish embryos. (**a**) Transgenic embryos expressing the EGFP-actin in their germ cells were injected with the mRNA coding for the F-actin marker Lifeact-Ruby targeted to the germ cells. Colocalisation of the two markers indicates that the actin brushes are composed of F-actin. Scale bar: 10μm. (**b**) *rac*1 and *rho*A RNAs are expressed uniformly at early stages of zebrafish embryogenesis. Whole mount *in situ* hybridisation using a *rac*1 (upper panels) and *rhoA* (lower panels) reveal ubiquitous expression of both RNAs during the stages at which germ cells migrate towards their target. Scale bar: 200μm.

© 2010 Macmillan Publishers Limited. All rights reserved.

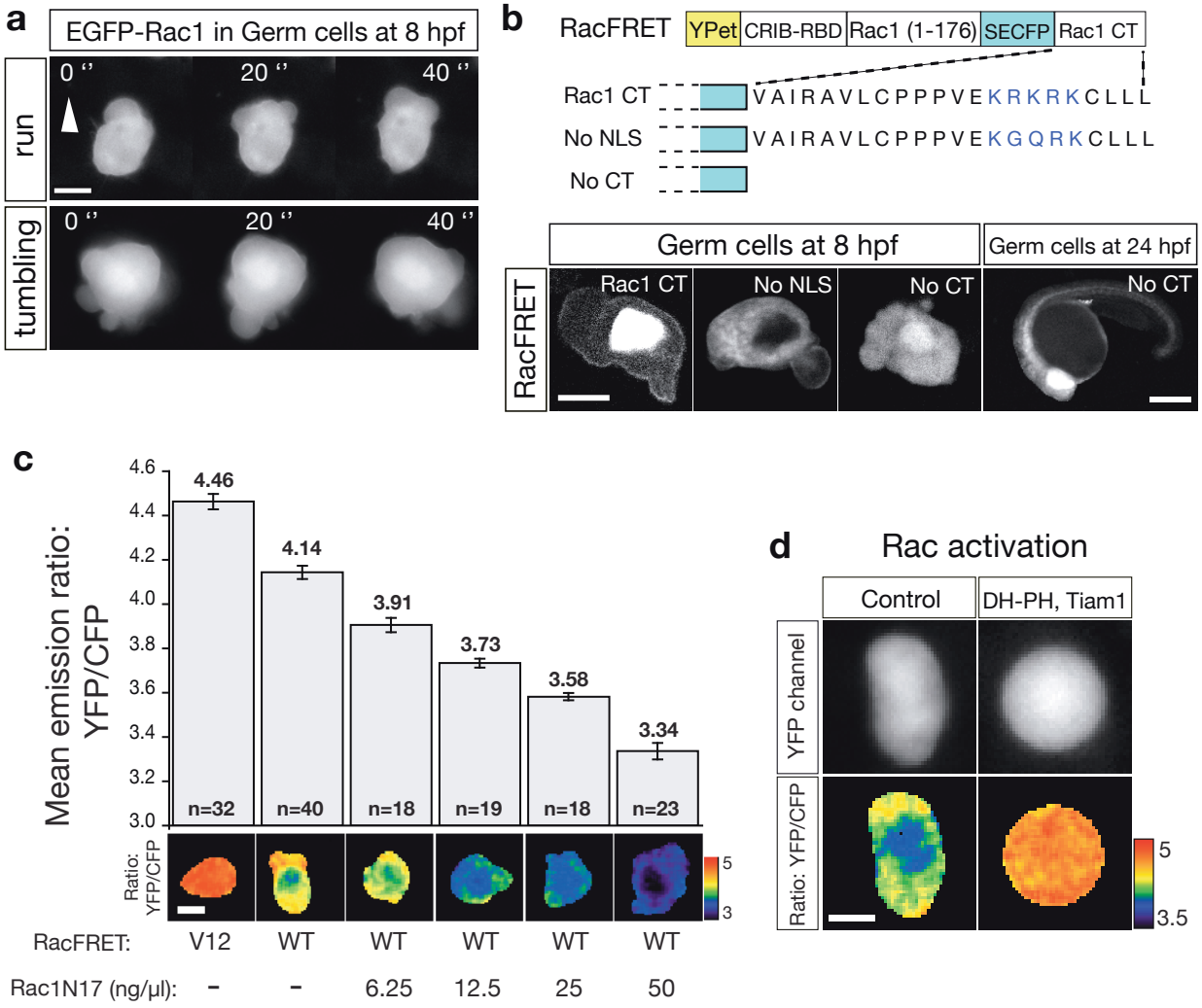

© 2010 Macmillan Publishers Limited. All rights reserved.

Figure S2 FRET-based imaging setup for measuring Rac activity in germ cells (**a)** Germ cells expressing EGFP-Rac1 were imaged at 8 hours post fertilisation (hpf). Migrating germ cells show uniform subcellular localisation of the protein during run (upper panels) and tumbling (lower panels) phases. (**b)** The domain structure of RacFRET biosensors and confocal images of the subcellular localisation of these biosensors in germ cells. The scheme shows the RacFRET domain structure and the amino acid sequence of the C-terminal (CT) domain of the biosensor that define the subcellular localization of the molecule. The original FRET construct [1] was sequestered in the nucleus (left panel). In an effort to match the subcellular localization of the RacFRET biosensor with that of the EGFP-Rac1 fusion (shown in a), two modifications were introduced into the C-terminal domain of the biosensor. To eliminate the nuclear localisation, the nuclear localization signal (NLS) was mutated by substituting KRKRK with KGQRK to give the 'no NLS' version. The other modification was a deletion of the 20 C-terminal residues of the biosensor (No CT). The FRET construct chosen for further work was the 'No CT' version since it exhibited more uniform distribution that resembles that of the Rac1 protein in a. Germ cells expressing the cytosolic RacFRET biosensor arrive at the migration target in a 24-hpf embryo suggesting that RacFRET biosensor does not interfere with signalling events relevant for germ cell migration (right panel). **(c)** A graph showing the differences between active and inactive states of the RacFRET biosensor. One-cell stage wild type embryos were injected with mRNA encoding for a RacFRET biosensor containing the G12V substitution within the biosensor (left cell) or with the mRNA encoding for the RacFRET biosensor (the rest of the cells). To achieve various activation states for RacFRET biosensor, different concentrations (as indicated below the graph) of mRNA encoding for the dominant-negative version of Rac1, $Rac1^{N17}$, were coinjected with the RacFRET biosensor. FRET imaging was performed at 8 hpf and mean emission ratio YFP/CFP values for the entire cell were plotted. **(d)** DH-PH domain of Tiam1, Rac guanine nucleotide-exchange factors (GEF), activates RacFRET biosensor. To demonstrate that the RacFRET sensor responds to specific GEFs, one-cell stage embryos were injected with the mRNA encoding for RacFRET biosensor together with the control (left panel) or with the mRNA encoding for the DH-PH domain of Tiam1 (right panel). **(e)** Time-dependent increase in RacFRET signal within the embryo. This increase is also observed when measuring FRET from a YPet-SECFP tandem **(f)**, indicating the non-specific nature of this effect and implying that FRET measurements using such biosensors should be compared within the same time window. 'n' signifies the number of cells examined. Scale Bars: 10μm for high magnification images, 300μm for low magnification image. Constructs used: *EGFP-zRac1-nos-3'UTR* (858) shows Rac localization in germ cells and was injected at 150pg per embryo. *RacFRET-X-nos-3'UTR* (517) is a RacFRET biosensor[1]. The RNA was injected at 360pg per embryo. *RacFRET-YPet-noNLS-nos1-3'UTR* (A563) is a modified RacFRET biosensor. The Venus in the original RacFRET[1] was replaced with YPet [2] and the nuclear localization signal in the C-terminal domain that follows SECFP was mutated with R185 to G and K186 to Q substitutions (these amino acids correspond to those found in the C-terminal domain of Zebrafish Rac1). The RNA was injected at 360pg per embryo. *RacFRET-YPet-noCT-nos1-3'UTR* (A422) is a modified cytosolic RacFRET biosensor. The Venus in the original Rac FRET [1] was replaced with YPet [2] and the C-terminal domain that follows SECFP in the original FRET construct was removed. The RNA was injected at 360pg per embryo. *RacV12FRET-YPet-noCT-nos1-3'UTR* (A569) served as a positive control for the cytosolic RacFRET biosensor. The G12 to V substitution was introduced into the Rac coding region of the biosensor. The RNA was injected at 360pg per embryo. *Rac1N17-nos1-3'UTR* (482) encodes the zebrafish dominant-negative $Rac1^{N17}$ version. *zTiamDH-PH-nos1-3'UTR* (A021) contains DH-PH domain of zebrafish Tiam1. The RNA was injected at 300pg per embryo. *YPet-10aa-SECFP-nos1-3'UTR (A615)* encodes the tandem fusion of YPet and SECFP linked by 10 amino acid. The RNA was injected at 300pg per embryo.

© 2010 Macmillan Publishers Limited. All rights reserved.

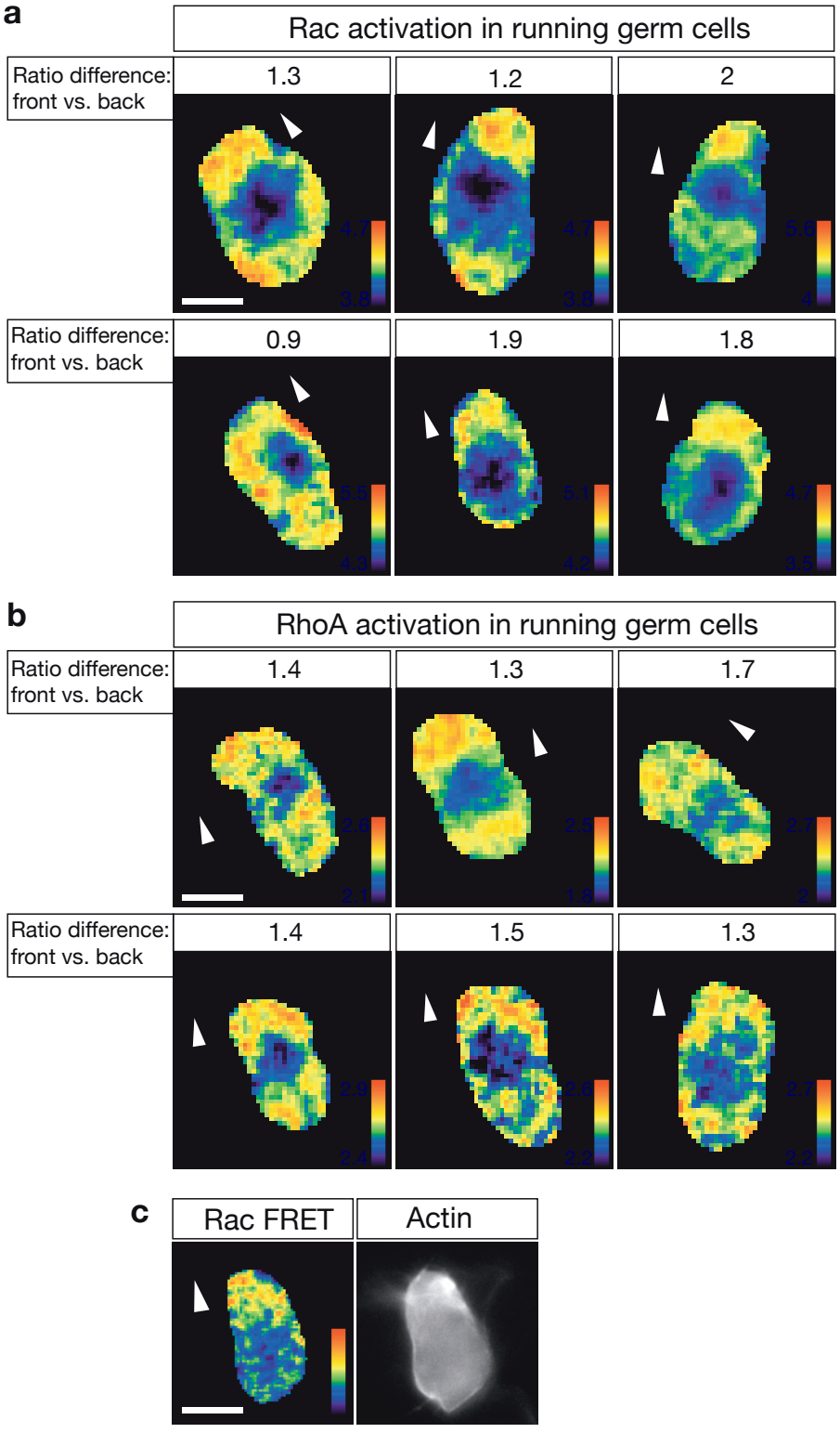

Figure S3 Rac and RhoA activation pattern measured by FRET. Multiple examples for Rac **(a)** and RhoA **(b)** activation pattern as measured in different migrating germ cells. Numbers above the images correspond to the ratio of activation at the front of the cell as compared to that at the back. Activation levels at the front and at the back were normalized with the low FRET signal in the nucleus that corresponds to the inactive state of the FRET biosensor. Arrow indicates the direction of a migration. (**c**) Rac1 activation (left image) and actin brushes (right image) localize to the front of a migrating germ cell. Embryos at one-cell stage were injected with the mRNA encoding for the RacFRET biosensor and with the mRNA encoding for the Lifeact-Ruby. FRET was measured in a migrating germ cell and then localisation of Lifeact was determined in the red channel (right image). Scale bar: 10μm.

© 2010 Macmillan Publishers Limited. All rights reserved.

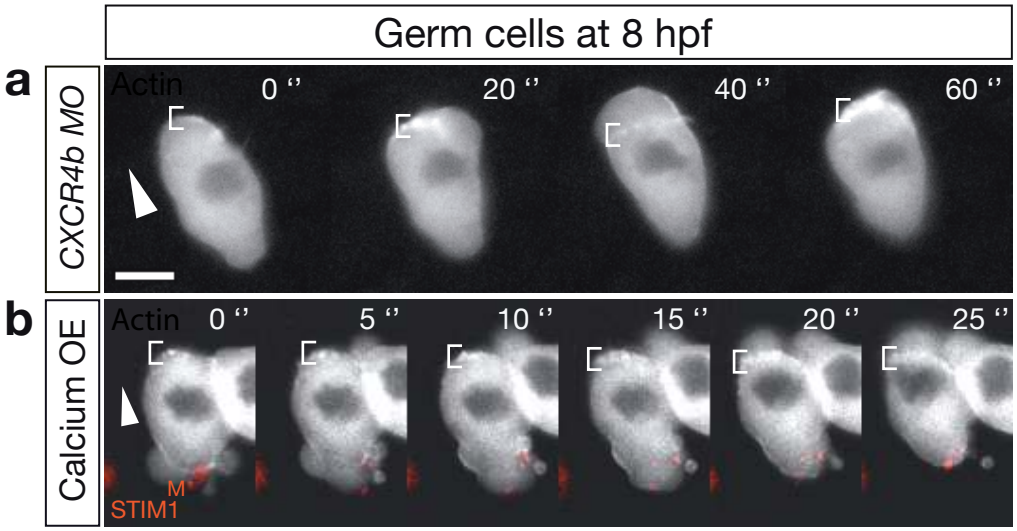

Figure S4 Actin brushes are formed independently of CXCR4b signalling and are not induced by the calcium rise at ectopic locations. **(a)** Actin dynamics in germ cells lacking CXCR4b signalling as a result of morpholino-mediated knock down of CXCR4b. The brackets demarcate the region of the actin brushes at the front of the cell, where normal appearance of actin brushes is seen. **(b)** Actin dynamics in germ cells, where ectopic calcium rise is induced. To increase calcium at ectopic locations, one–cell stage embryos expressing EGFP-Actin in germ cells were injected with mRNA encoding for $STIM1^{M}$ mutant[3], which results in formation of blebs induced at ectopic sites where $STIM1^{M}$ is localized (red). Actin brushes were not observed in those sites. Arrowheads indicate the direction of a migration. Scale bar: 10μm.

© 2010 Macmillan Publishers Limited. All rights reserved.

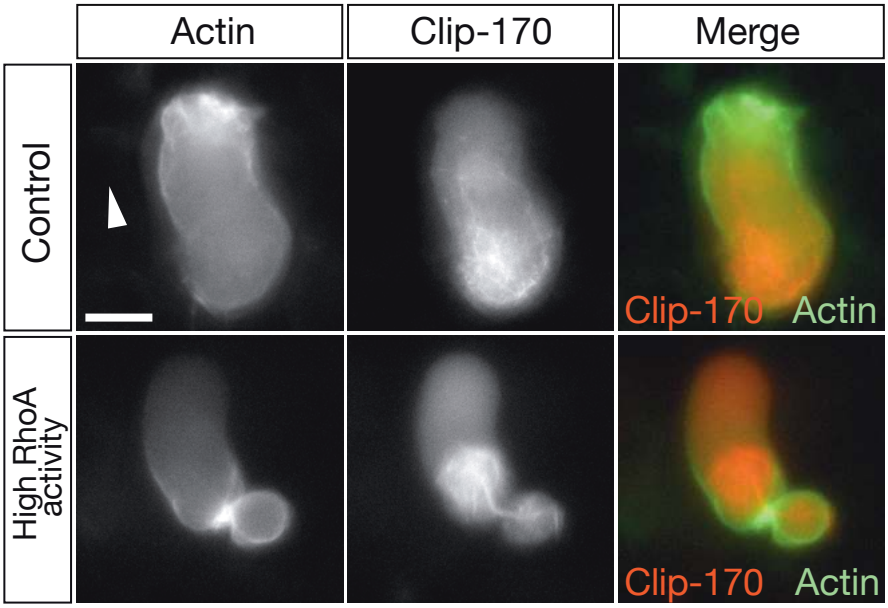

Figure S5 Increased RhoA activity results in actin recruitment to the back of the germ cells. One-cell stage embryos were injected with the mix of mRNAs encoding for Lifeact-Ruby, Clip-170-EGFP and control or the activated RhoA version, $RhoA^{V14}$. The Clip-170-EGFP fusion protein labels the MTOC and the microtubules emanating from it are localised to the back of non-manipulated migrating germ cells (labelled in red in the figure), while actin (labelled in green in the figure) is observed at the cell front. In cells in which RhoA activity is elevated, actin is observed at the back of the cells, a region marked by Clip-170. Arrow indicates the direction of a migration. Scale bar: 10µm. Constructs used: *GFP-clip-170-nos1-3'UTR* (779) contains the human *clip-170* gene fused to GFP[4]. The RNA was injected at 300pg per embryo.

© 2010 **Macmillan Publishers Limited. All rights reserved.**

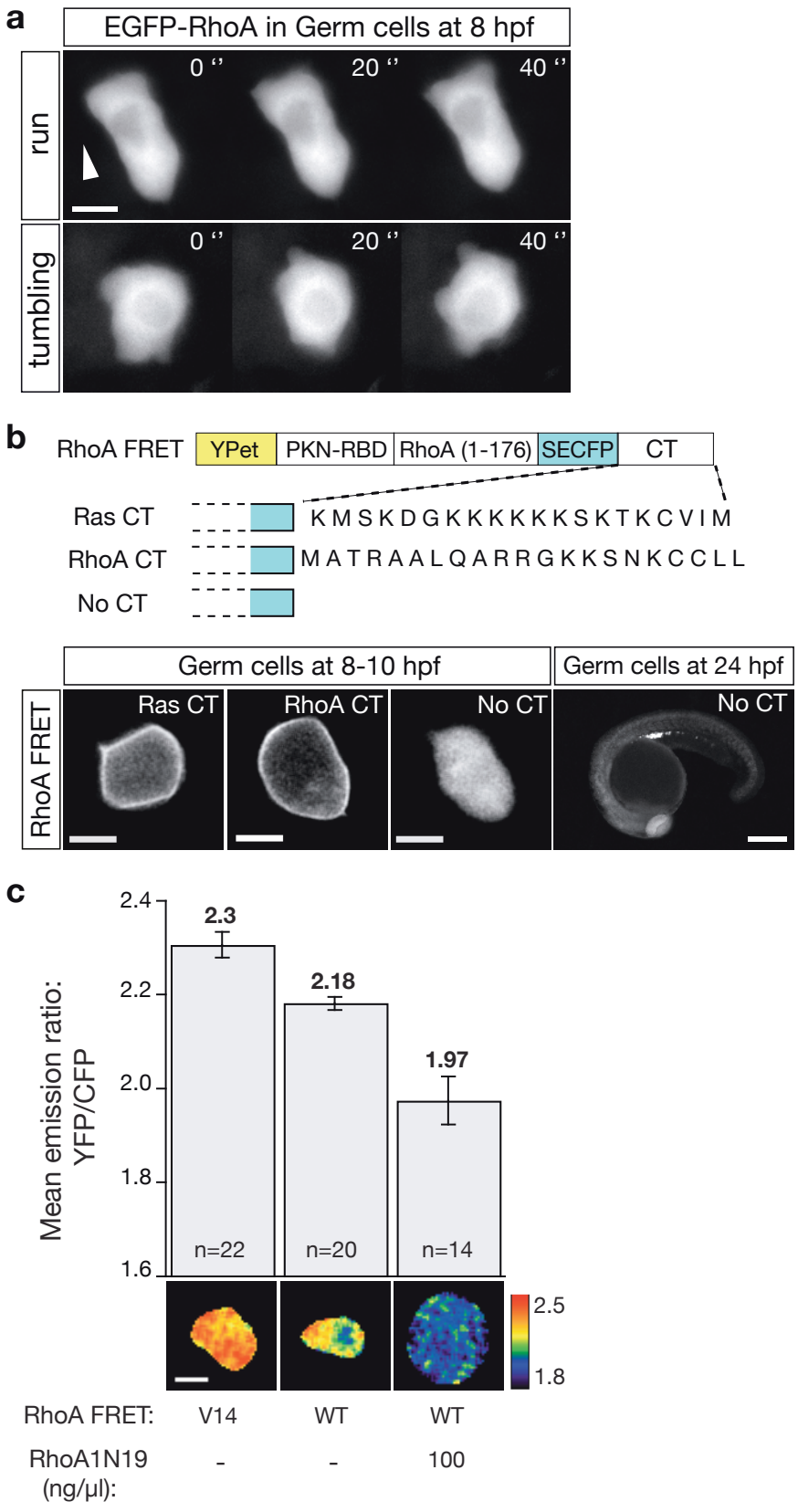

© 2010 Macmillan Publishers Limited. All rights reserved.

Figure S6 Subcellular localization of RhoA and RhoA FRET biosensor in germ cells. (**a)**. Snap-shots from movies recording EGFP-RhoA-expressing germ cells show subcellular localization of RhoA during run (upper panel) and tumbling (lower panel) phases. **(b)** The domain structure of RhoA FRET biosensors and the subcellular localization of the biosensors in germ cells. The scheme shows the domain structure of the modified RhoA FRET biosensors including the fluorophores, the RhoA sequences, protein kinase N-Rho binding domain (PKN-RBD) and the amino acid sequence of the C-terminal (CT) domain of the protein. Confocal images of germ cells expressing the various biosensors show the subcellular localization of the RhoA FRET construct containing the Ras C-terminal domain[5] (left image, Ras CT), the C-terminal modification to the original RhoA FRET construct, in which the Ras C-terminal sequence was replaced with that of the zebrafish RhoA (RhoA CT) and the 'No CT' RhoA FRET biosensor, in which the last 20 C-terminal amino acids were deleted (No CT). The distribution of the 'No CT' protein resembles that observed for the EGFP-RhoA in panel a, and therefore this version was further used for FRET measurements. Germ cells expressing the 'No CT' cytosolic RhoA FRET biosensor arrive at their migration target in 24 hpf embryos (right) suggesting that RhoA FRET biosensor does not interfere with signalling events relevant for germ cell migration. **(c)** A graph showing the differences between active and inactive states of the 'No CT' RhoA FRET biosensor. Wild type embryos at one-cell stage were injected with mRNA encoding for a RhoA FRET biosensor containing the active form with the G12V substitution within the biosensor (left cell), with the mRNA encoding for the RhoA FRET biosensor (middle cell), or with the mix of mRNAs encoding for the RhoA FRET biosensor and two dominant negative RhoA isoforms (RhoAa and RhoAc) containing the T19N substitution. The cell expressing the dominant-negative RhoA version on the right appears larger as such cells exhibit cytokinesis defects (MRF, unpublished observations). 'n' signifies the number of cells examined. Scale Bars: 10µm for high magnification images, 300µm for low magnification image. Constructs used: *EGFP-zRhoA-nos-3'UTR* (860) shows the localization of the zebrafish RhoA in germ cells and was injected at 150pg per embryo. *RhoA FRET-X-nos-3'UTR* (519 is the original RhoA FRET biosensor with the C-terminal domain of Ras[5]. The RNA was injected at 360pg per embryo. *RhoA FRET-YPet-RhoA CT-nos-3'UTR* (A861) is a modified RhoA FRET biosensor. The Venus in the original RhoA FRET [5] was replaced with YPet [2] and the most C-terminal domain of Ras that follows SECFP in the original FRET construct, was replaced with that of the Zebrafish RhoA. The RNA was injected at 360pg per embryo. *RhoA FRET-YPet-nos1-3'UTR* (A676) is a modified RhoA FRET biosensor. The Venus in the original RhoA FRET [5] was replaced with YPet [2] and the most C-terminal domain that follows SECFP in the original FRET construct was removed. The RNA was injected at 360pg per embryo. *RhoA-V14-FRET-YPet-nos1-3'UTR* (A766) served as a positive control for the modified RhoA FRET biosensor. The G12 to V substitution was introduced in the RhoA coding region of *RhoA FRET-YPet-nos1-3'UTR*. The RNA was injected at 360pg per embryo. *RhoAa N19-nos1-3'UTR* (780) encodes the zebrafish dominant-negative RhoA^{N19} version of RhoA isoform *a*. The RNA was injected at 360pg per embryo. *RhoAc N19-nos1-3'UTR* (509) encodes the zebrafish dominant-negative RhoA^{N19} version of RhoA isoform *c*. The RNA was injected at 360pg per embryo.

© 2010 Macmillan Publishers Limited. All rights reserved.

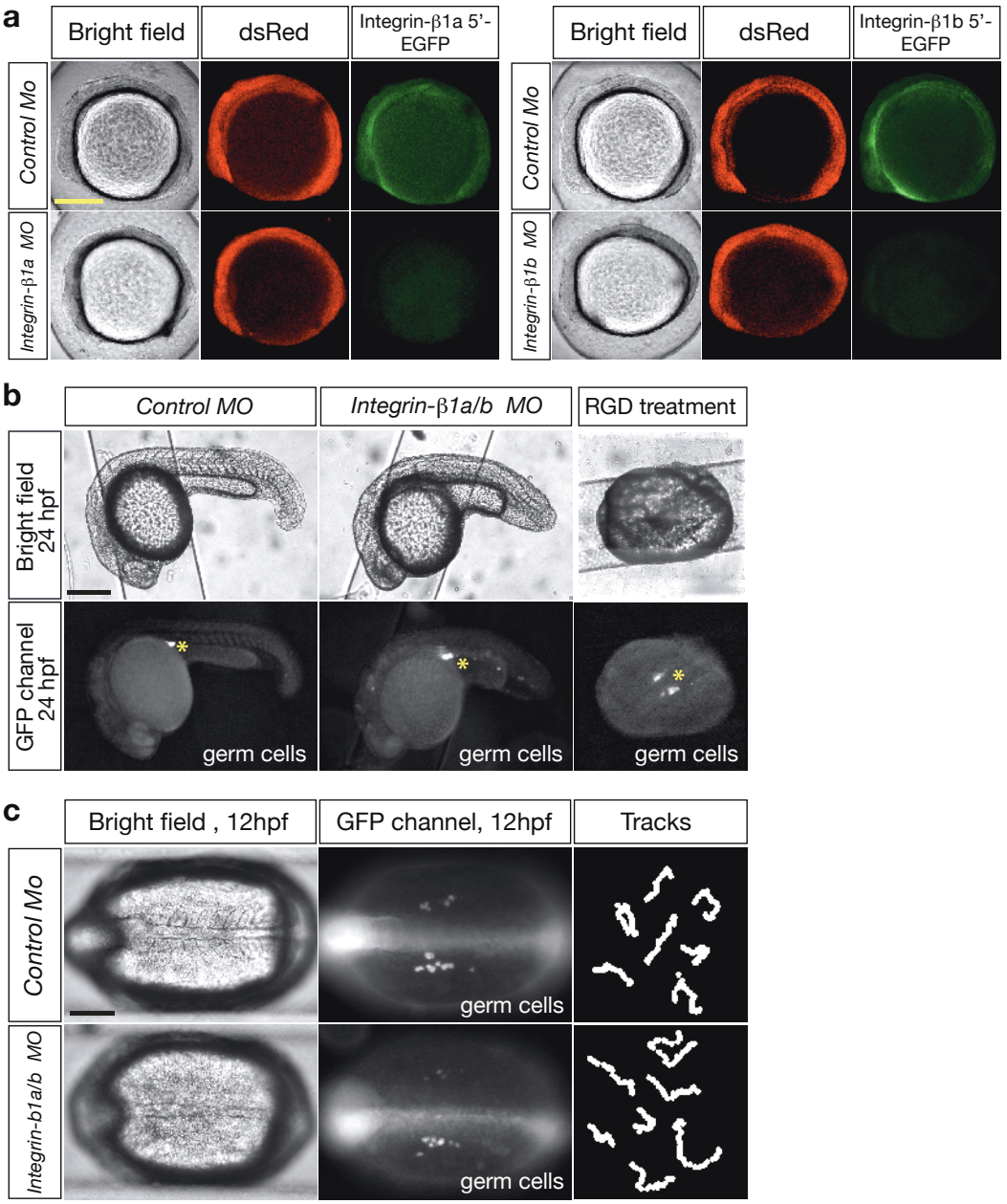

Figure S7 Role of ECM in germ cell migration. **(a**) The efficiency of anti integrin-β1a and integrin-β1b morpholinos was tested using the EGFP fusions of 5' regions of integrin-β1a and integrin-β1b. Embryos at one-cell stage were injected with the mix of the mRNAs encoding for the respective isoforms of integrin-β1 5'-EGFP fusion and mRNA encoding the dsRed control together with the control morpholinos or anti integrin-β1 morpholinos (integrin-β1a in the left panel and integrin-β1b in the right panel). Morpholinos used: integrin-β1a: 5' TATGAAAAGTAGCTTCAGGTCCATC 3' and integrin-β1b: 5' AATCAGGAGCAGCCTTACGTCCATC 3' (2ng per embryo each). A complete inhibition of translation of the RNA containing the integrin sequence is observed (bottom right panels in a) **(b**) Lateral view of the 24 hpf embryos imaged in the bright field (upper panels) or in the fluorescent GFP channel (lower panels) to visualize the germ cells. The embryos were injected at the one-cell stage with control morpholinos (left panel), with the mix of anti integrin-β1a and integrin-β1b morpholinos used in panel a (middle panel), or incubated with 1mM RGD peptide (Sigma G1269) starting from the 256-cell embryonic stage. Despite the adverse effect on somatic development of the treatments (short body axis and defects in formation of somatic boundaries), the germ cells correctly arrive at their target (marked with an asterisk). **(c)** Detailed analysis of germ cells migration in embryos in which integrin-β1a and integrin-β1b function were knocked down (as in panel a). In the integrin-β1a/b morphants, the germ cells arrive at their intermediate target at 12 hours post fertilization forming two clusters on both sites of the notochord (middle panel), similar to cells in control embryos. The germ cells migrating in the embryos knocked down for integrin-β1a/b function generate tracks of similar length (70 minutes recorded at 8 hpf) to those of control cells and thus migrate at a comparable speed (right panel). Scale Bar: 300μm. Constructs used: Integrin-β1a-5' EGFP contains the 5' region of the Integrin-β1a mRNA that includes the morpholino binding site fused to EGFP. The RNA was injected at 300pg per embryo. Integrin-β1b-5' GFP contains the 5' region of the Integrin-β1b mRNA that includes the morpholino binding site fused to EGFP. The RNA was injected at 300pg per embryo.

© 2010 Macmillan Publishers Limited. All rights reserved.

Supplementary Movie Legends

Movie S1 Actin dynamics in a germ cell during run and tumbling phases. A germ cell expressing EGFP-actin was imaged during the developmental stage at which germ cells normally migrate. Frames were captured every 5 sec using a Zeiss Axioplan2 microscope and the movie plays at 12 frames/sec.

Movie S2 Actin dynamics in a germ cell with reduced Rac activity. The germ cell expressing EGFP-actin and CRIB-RasCT was imaged during the developmental stage at which germ cells normally migrate. Frames were captured every 5 sec using a Zeiss Axioplan2 microscope and the movie plays at 12 frames/sec.

Movie S3 Actin dynamics in a germ cell with increased Rac activity. The germ cell expressing EGFP-actin and $Rac1^{V12}$ was imaged during the developmental stage at which germ cells normally migrate.. Frames were captured every 5 sec using a Zeiss Axioplan2 microscope and the movie plays at 12 frames/sec.

Movie S4 Rac activation pattern in a migrating germ cell during run phase is presented as a color-coded YFP/CFP emission ratio. A germ cell expressing RacFRET sensor was during the developmental stage at which germ cells normally migrate . Frames of the CFP and YFP emission channels were captured sequentially every 20 sec using the switching wheel in a Zeiss Axioplan2 microscope and the movie plays at 3 frames/sec.

Movie S5 Rac activation pattern in a migrating germ cell during tumbling phase is presented as a color-coded YFP/CFP emission ratio. A germ cell expressing RacFRET sensor was imaged during the developmental stage at which germ cells normally migrate. Frames of the CFP and YFP emission channels were captured sequentially every 5 sec using the switching wheel in a Zeiss Axioplan2 microscope and the movie plays at 12 frames/sec.

Movie S6 Actin dynamics in germ cell migrating non-directionally in the absence of CXCR4b signalling. A germ cell expressing EGFP-actin in the embryo where CXCR4b expression was inhibited by anti-CXCR4b morpholinos was imaged during the developmental stage at which germ cells normally migrate . Frames were captured every 5 sec using a Zeiss Axioplan2 microscope and the movie plays at 12 frames/sec.

Movie S7 Actin dynamics in germ cell with reduced RhoA activity. A germ cell expressing EGFP-actin and YFP-PKN-RasCT was imaged during the developmental stage at which germ cells normally migrate . Frames were captured every 5 sec using a Zeiss Axioplan2 microscope and the movie plays at 12 frames/sec.

Movie S8. Actin dynamics in germ cell with elevated RhoA activity. A germ cell expressing EGFP-actin and $RhoA^{V14}$ was imaged during the developmental stage at which germ cells normally migrate . Frames were captured every 5 sec using a Zeiss Axioplan2 microscope and the movie plays at 12 frames/sec.

Movie S9. The behaviour of isolated germ cells plated in Matrigel. Cell membranes are labelled with EGFP and frames were captured every 2 sec using a Zeiss Axioplan2 microscope. The movie plays at 30 frames/sec.

Movie S10. Actin dynamics in a germ cell migrating through the somatic environment within the developing embryo. Actin in the germ cell is visualised with Lifeact-EGFP and the membranes in all cells are visualized with farnesylated mCherry. Frames were captured every 5 sec using a Zeiss Axioplan2 microscope and the movie plays at 12 frames/sec.

Movie S11. Expression of actin (left) and E-cadherin (right) in migrating germ cells. Actin in the germ cell is visualised with Lifeact-Ruby and E-Cadherin with E-cadherin-GFP fusion. Frames were captured every 5 sec using a Zeiss Axioplan2 microscope and the movie plays at 12 frames/sec.

Movie S12. Actin (left) and E-cadherin (right) co-localise at the back of a germ cell upon enhanced RhoA activity. A germ cell expressing Lifeact-Ruby that labels actin, E-cadherin-GFP and $RhoA^{V12}$ was imaged during the developmental stage at which germ cells normally migrate. Frames were captured every 5 sec using a Zeiss Axioplan2 microscope and the movie plays at 12 frames/sec.

Movie S13. Actin dynamics and inhibition of migration in a germ cell expressing the dominant negative form of E-cadherin that is lacking extracellular domains 1 and 2 (D-EC1-2). A germ cell expressing D-EC1-2 was imaged during the developmental stage at which germ cells normally migrate . Actin in germ cells is visualised with Lifeact-EGFP and the membranes in all cells are visualized with farnesylated mCherry. Frames were captured every 5 sec using a Zeiss Axioplan2 microscope and the movie plays at 12 frames/sec.

Movie S14. Actin dynamics and inhibition of migration in germ cells in embryos injected with low levels of anti *E-cadherin* morpholinos. The cells were imaged during the developmental stage at which germ cells normally migrate. Actin is visualised with Lifeact-EGFP and the membranes in all cells are visualized with farnesylated mCherry. The germ cell is able to polarize, form blebs and actin brushes, which exhibit retrograde flow. Frames were captured every 5 sec using a Zeiss Axioplan2 microscope and the movie plays at 12 frames/sec.

Movie S15. Actin dynamics and inhibition of migration in germ cells in embryos injected with high levels of anti *E-cadherin* morpholinos. The cells were imaged during the developmental stage at which germ cells normally migrate. Actin is visualised with Lifeact-EGFP and the membranes in all cells are visualized with farnesylated mCherry. The germ cells are unable to polarize and actin brushes formation is distorted. Frames were captured every 5 sec using a Zeiss Axioplan2 microscope and the movie plays at 12 frames/sec.

References:

1. Itoh, R.E. *et al.* Activation of rac and cdc42 video imaged by fluorescent resonance energy transfer-based single-molecule probes in the membrane of living cells. *Mol Cell Biol* **22**, 6582-6591 (2002).
2. Nguyen, A.W. & Daugherty, P.S. Evolutionary optimization of fluorescent proteins for intracellular FRET. *Nature biotechnology* **23**, 355-360 (2005).
3. Blaser, H. *et al.* Migration of zebrafish primordial germ cells: a role for Myosin contraction and cytoplasmic flow. *Developmental cell* **11**, 613-627 (2006).
4. Perez, F., Diamantopoulos, G.S., Stalder, R. & Kreis, T.E. CLIP-170 highlights growing microtubule ends in vivo. *Cell* **96**, 517-527 (1999).
5. Yoshizaki, H. *et al.* Activity of Rho-family GTPases during cell division as visualized with FRET-based probes. *The Journal of cell biology* **162**, 223-232 (2003).

© 2010 **Macmillan Publishers Limited. All rights reserved.**